JOURNAL OF CATALYSIS 129, 368–382 (1991)

Homologation of Propene with Methane Using Nickel-Supported Catalysts: A Surface Characterization Study

CESAR OVALLES, VLADIMIR LEON, SHEILA REYES, AND FRANCISCO ROSA

Petrochemical Department, INTEVEP S. A., Apdo.76343 Caracas 1070A, Venezuela

Received March 20, 1990; revised September 4, 1990

The homologation of propene with methane was studied using alumina- and silica-supported nickel catalysts. The catalysts were activated under a methane flow previous to the reaction. Experiments carried out in a propene/methane mixture at 350°C showed that the Ni/SiO_2 system was more active for the homologation reaction (81.4% selectivity to butanes) than its alumina analog (6.2% selectivity to C_4 compounds). From control experiments carried out under a nitrogen atmosphere and in a hydrogen-activated catalyst, it was concluded that the methane molecule incorporates into the hydrocarbon chain. The XPS studies showed the presence of carbonaceous species (but not necessarily graphitic) on the catalytic surfaces. The concentration in the silica catalyst was higher than that in its alumina analog, suggesting that, most probably, these species were involved as intermediates in the propene homologation reaction. The silica-based catalyst showed higher metal dispersion than that found in its alumina counterpart. This can be attributed to the formation of $NiAlO_4$ on the catalyst surface, which can also explain the lower activity observed for butane production. On the basis of the experimental evidence, a propene homologation mechanism can be proposed which involves the reaction of methane with the metal to generate CH_x species (where $x = 0, 1, 2,$ or 3), which in turn react with propene, producing the homologation products (butanes).

INTRODUCTION

In the past few years, the reactions of transformation of methane into more valuable products have been the subject of study not only in heterogeneous (*1–4*) but in homogeneous catalysis (*3–5*). In particular, the reactions between natural gas (methane) and hydrogen acceptor molecules, i.e., olefins, are thermodynamically favored (Eqs. (1) and (2)) and represent an interesting route for the industrialization of this natural resource.

$$CH_4 + C_2H_4 \rightarrow$$

	$\Delta G°$ (kcal/mol)	
$CH_3CH_2CH_3$	−3.2	(1)

$$CH_4 + C_3H_6 \rightarrow \tfrac{1}{2}CH_3CH_2CH_2CH_3 + \tfrac{1}{2}(CH_3)_3CH \qquad -0.21 \qquad (2)$$

Reactions (1) and (2) are commonly known as homologation reactions mainly because the final product has one more carbon atom than the starting olefin. In particular, Schleyer and co-workers (*6*) reported that methane reacted with benzene, cyclopentene, and propene to produce small amounts of toluene, methylcyclopentane, and butanes, respectively, using silica-supported nickel catalysts. The catalyst had to be reduced in methane in order to be active for the homologation reaction, and a surface methane–nickel species formed during the reduction period is proposed as an intermediate in the reactions. However, there are no characterization studies nor comparisons with the hydrogen-activated catalysts.

Sodesawa and co-workers (*7*) reported oxidative methylation of propene with methane to butanes in the presence of oxygen using a 3% Na_2O/La_2O_3 catalyst. A maximum 10.1% yield of C_4 compounds was obtained. No details regarding the reaction mechanism were given. Scurrel reported (*3, 8*) that a mixture of methane and ethylene reacted over sulfated-treated zirconia cata-

0021-9517/91 $3.00

lysts to produce higher hydrocarbons at 300°C. In the beginning of the experiment, the ethylene and methane conversions were high (80–90 and 17–58%, respectively) but at the end, the selectivity changed to higher hydrocarbons. The product distribution varied considerably in the absence of methane, suggesting that the presence of methane exerted a decided effect on the catalytic behavior. It is concluded that the catalysts interacted very strongly with methane (probably due to its superacidity behavior), and a direct methane–ethylene coupling is proposed (*8*) in order to explain the generation of homologation products.

Osada *et al.* (*9*) reported the oxidative methylation of toluene with methane over alkali-promoted Y_2O_3–CaO catalysts to give ethylbenzene and styrene. The order of selectivity to higher hydrocarbons is Li > Na > K. By comparison with the results of the oxidative coupling of methane to ethane/ethylene a mechanism for the methylation of toluene is proposed and involves the reaction between the benzyl and the methyl radicals, formed on the basic surface of the catalyst, to generate the methylated compounds.

In the literature (*6–9*), the lack of fundamental knowledge as well as catalyst characterization studies is evident. For this reason, we concentrate on understanding the mechanism of methane activation during the homologation of propylene to butanes using nickel-supported catalysts. The metal is supported over alumina and silica and the resulting catalysts are characterized by TPR, XPS, and magnetic susceptibility techniques. Finally, the most probable mechanism for the homologation reaction is proposed.

EXPERIMENTAL

The methane, propylene, and helium were supplied by Matheson. Nitrogen was purchased from Gases Industriales de Venezuela. The alumina was obtained from AKZO with a surface area of 274 m^2/g, pore volume of 0.69 ml/g, and mesh granules of 80–100. The silica was purchased from Grace Davison with a surface area of 612 m^2/g, pore volume of 0.33 ml/g, and mesh granules of 80–100.

For the analysis of the reaction effluents, a Varian 3700 gas chromatograph equipped with a FID detector is used and a standard mixture (prepared using a Matheson gas blender unit) is used for calibration purposes. A Hewlet–Packard Model 3390A integrator is employed, and the identification and quantification of the products are performed by the external standard method.

XPS measurements are made with the surface analysis system from Leybold–Heraeus (EA-11) at INTEVEP, which is operated with a magnesium anode (1253.6 eV). Pass energy is 200 eV and the data acquisition and manipulation are performed using an HP-1000 computer on-line with the equipment. The sensitivity factor is calculated using the method reported by Leon and Carrazza (*10*).

The magnetic susceptibility measurements are made in a Cahn electrobalance equipped with a magnet, a vacuum system, and gas distribution lines. The calculations are done using the procedure reported by Sinfelt and Carter (*11*).

The temperature-programmed reduction (TRP) experiments are carried out by placing a sample of fresh catalyst in a $\frac{1}{4}$-in. glass tube, which is then placed inside an oven and coupled to a thermal conductivity detector. The catalyst is contacted with a mixture of 20% of methane in nitrogen and is heated from room temperature to 1000°C at 10°C/min.

Preparation of the Catalysts

The nickel-supported catalysts are prepared using the incipient wetness technique. Six milliliters of a 4 *M* solution of Ni $(NO_3)_2 \cdot 6H_2O$ (Aldrich) is added and mixed with 20 g of silica for 2 h. For preparation of the alumina analog, 13.8 ml of a 2 *M* solution is used for 20 g of Al_2O_3. The catalysts are dried at 150°C for 2 h and calcined at 600°C in air overnight. The nickel con-

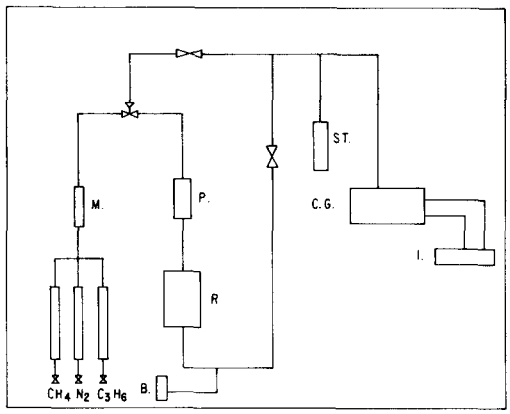

FIG. 1. Experimental apparatus used in the homologation reaction (M, gas mixer; P, preheater; ST, gas standard for calibration purposes; R, reactor; B, gas bubbler; CG, gas chromatograph; I, plotter–integrator).

tents are determined to be 7.19 and 7.49%, with surface areas of 318 and 211 m^2/g for the silica and the alumina catalysts, respectively.

Catalytic Reactions

The catalytic system used in this work is shown in Fig. 1. It consists basically of three sections, a mass flow control unit, the reactor, and the analysis system. A 0.62-g amount of the catalyst (dispersed in 0.5 g of carburundum) is placed in a $\frac{3}{8}$-in-internal-diameter stainless-steel reactor with an internal volume of 1 cm^3. The catalyst is activated by passing 10 cm^3/min flow of methane at 600°C for 8 h. In order to purge the system, a flow of nitrogen is used until the reactor reaches room temperature. The reaction mixture of 9% of propene in methane is passed and the reactor is heated to the desired temperature. Several samples are taken and analyzed on-line until the system reaches a stationary state (approx 1 h). All the experiments are carried out under ambient pressure.

The study of the effects of the operating conditions (space velocity and temperature) on the nickel-supported catalysts and on the maximum production of homologation products (butanes) is reported elsewhere (*12*). For the alumina and silica catalysts GHSV values of 565 and 968 h^{-1} are used, respectively. The temperature for all experiments is 350°C.

For the reactions carried out in the absence of methane, a 9% mixture of propene in nitrogen is used. The activation protocol as well as the reaction conditions is the same as that for the methane reactions. The conditions for the activation in hydrogen atmosphere are 10 cm^3/min flow of H_2, 300°C for 8 h.

Characterization of the Catalysts

For the XPS measurements, on–off valves are connected at the entrance and exit of the reactor depicted in Fig. 1. After the activation procedure or the 1-h reaction period (propene and methane), the valves are closed and the reactor is placed in a nitrogen-filled dried box. The samples are then transferred to the ultrahigh vacuum chamber of the XPS equipment. The entire procedure is performed under a nitrogen atmosphere.

For the magnetic susceptibility measurements, a sample of 20 mg of the fresh catalyst is heated at 600°C under vacuum until it reaches constant weight. The sample is then reduced with 12 cm^3/min of methane at 600°C for 8 h. The magnetic susceptibility is measured at 298°K under vacuum and heated at 350°C in the presence of a mixture of 9% of propene in methane for 1 h. After the mixture is cooled to room temperature, the magnetic susceptibility is measured again.

RESULTS AND DISCUSSION

Activation of the Catalyst

Temperature-programmed reduction experiments are carried out in order to determine conditions suitable for the activation of the catalysts under a methane atmosphere; results are shown in Figs. 2 and 3. For the Ni/Al_2O_3 catalyst (Fig. 2), the first process is observed at 676 and at 623°C for the silica analog (Fig. 3). Generally, this process is associated with the reduction of the cata-

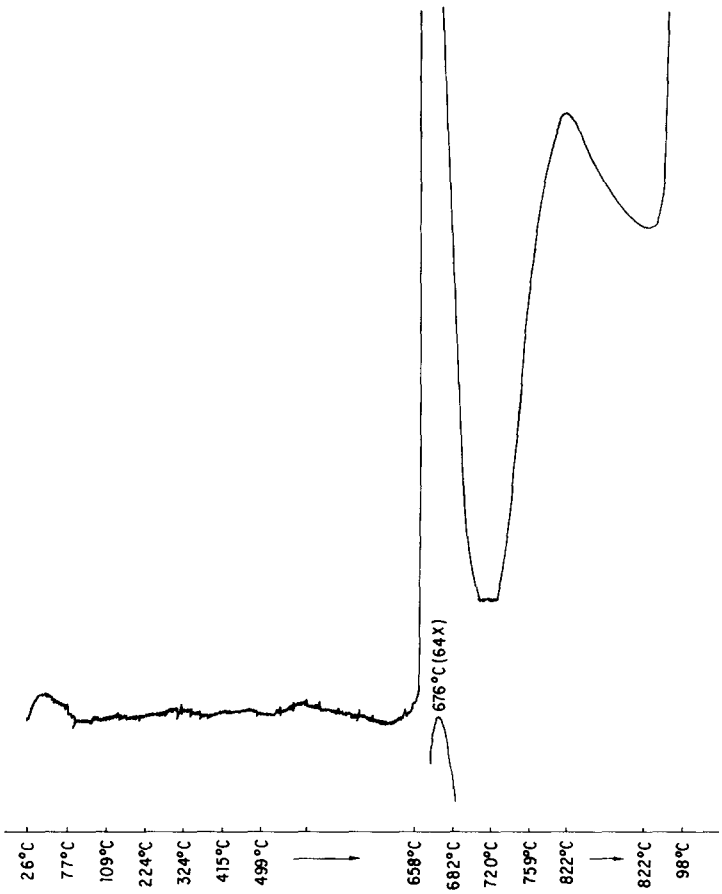

FIG. 2. Temperature-programmed reduction experiment for the Ni/Al_2O_3 catalyst using 20% methane–nitrogen mixture at 10°C/min.

lysts by methane and can be attributed to a carburization process (*13*). In order to avoid sintering, a lower temperature (600°C) is chosen for the catalyst activation, and to ensure complete reduction of the metal (confirmed by XPS), pure methane is used for a time period of 8 h.

Catalytic Reactions

The results of the homologation of propene using the Ni/Al_2O_3 catalyst are shown in Table 1. For this catalyst, the selectivity to butanes is 6.2% at 350°C and 565 h^{-1} employing a methane–propene mixture (Experiment 1). When methane is replaced by nitrogen (Experiment 2), the selectivity to C_4 remains approximately constant (5.8%), butane being the only homologation product (ratios iC_4/nC_4 and olefins/parafins equal to zero) and propane the major product (60.2 and 85.4% for Experiments 1 and 2, respectively). Therefore, the presence of methane has no effect on the production of homologation compounds, suggesting that the CH_4 molecule, most probably, does not incorporate into the hydrocarbon chain for the Ni/Al_2O_3 system. The formation of the small amounts of C_4H_8 can be attributed to self-homologation of propene similar to the results reported in the literature by several authors (*14–20*) in their metal-supported homologation studies.

For the Ni/SiO_2 catalyst a significant decrease in the butane production is observed

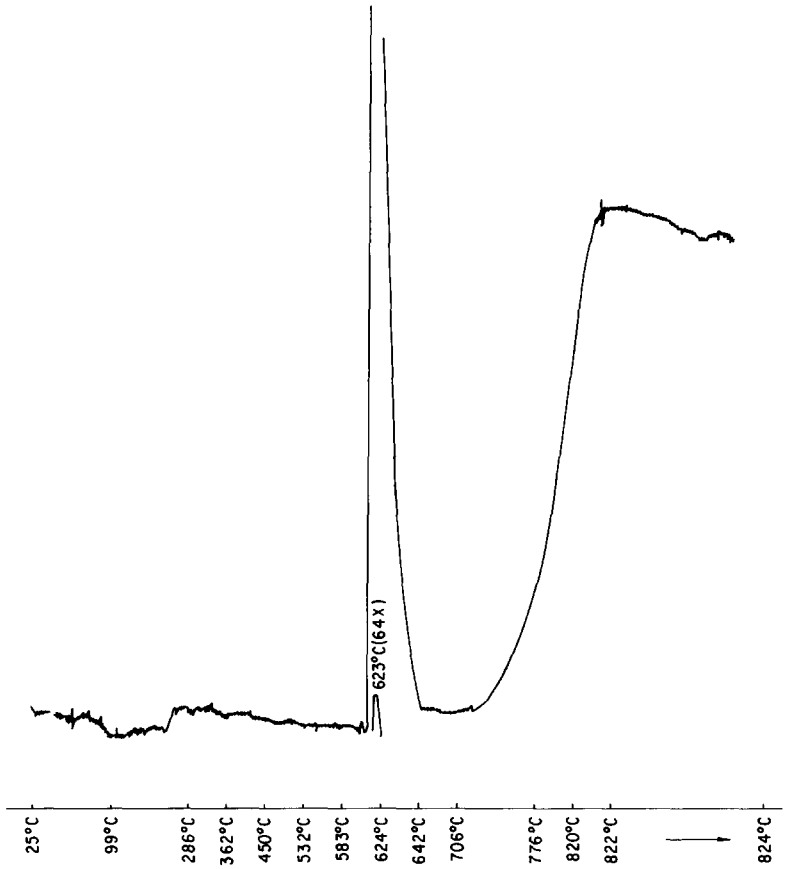

FIG. 3. Temperature-programmed reduction experiment for the Ni/SiO_2 catalyst using 20% methane–nitrogen mixture at 10°C/min.

by replacing the methane with nitrogen. Effectively, the butane selectivity diminishes from 81.4% in the methane–propene mixture (Experiment 3) to 2.2% in the nitrogen–propene feed (Experiment 4) under the same reaction conditions (350°C and 968 h^{-1}). According to Schleyer and co-workers (*6*), C_4 compounds obtained under a methane atmosphere are attributed to the formation of C_1 species present in the catalyst and formed during the activation period. These species react with propene to yield the homologation products. The methane present in the feed regenerates the C_1 species, covering the surface in order to complete the catalytic cycle. Circumstantial evidence of the previous mechanism is that the iC_4/nC_4 ratio is the same for both experiments (Experiments 3 and 4), suggesting similar pathways for the formation of the homologation products.

On the other hand, the olefin fraction decreased in the reaction carried out under nitrogen (Experiment 4) in comparison with that performed under methane (Experiment 3). This effect can be attributed to the partial removal of the carbonaceous material (C_1 species) in the former experiment which opens coordination sites for the hydrogenation of the unsaturated molecules. In the reaction carried out under methane, the concentration of the C_1 species is approximately constant and, therefore, fewer olefins are hydrogenated. This effect is also shown in the selectivity of propane which increases from 16.4% in the CH_4-containing experiment to 96.1% in the nitrogen-containing reaction.

For the nickel–silica catalyst reduced un-

TABLE 1

Product Distribution of the Reaction of Propene with Methane, Nitrogen, and Hydrogen Using Alumina- and Silica-Supported Nickel Catalysts

Expt	Catalyst	Reaction	% Con.[a]	% SC_2[b]	% SC_3[c]	% SC_4[d]	iC_4/nC_4[e]	Olef./Paraf.[f]
1	Ni/Al_2O_3[g]	$CH_4 + C_3H_6$	9.2	33.6	60.2	6.2	0.0	0.0
2	Ni/Al_2O_3[g]	$N_2 + C_3H_6$	8.7	8.8	85.4	5.8	0.0	0.01
3	Ni/SiO_2[h]	$CH_4 + C_3H_6$	4.7	2.2	16.4	81.4	0.2	4.0
4	Ni/SiO_2[h]	$N_2 + C_3H_6$	4.3	1.7	96.1	2.2	0.2	0.02
5	Ni/SiO_2[i]	$CH_4 + C_3H_6$	7.0	0.0	47.2	52.7	[j]	0.06
6	Ni/SiO_2[i,k]	$H_2 + C_3H_6$	7.2	19.3	48.4	32.3	0.1	2×10^{-3}

[a] Conversion with respect to propene in the gas feed (9% of C_3H_6 in CH_4, N_2, or H_2).

[b] Percentage of selectivity with respect to ethylene–ethane, moles of $C_2 \times 100$/total moles of products, ratio $C_2H_4/C_2H_6 > 10$.

[c] Percentage of selectivity with respect to propane, moles of $C_3 \times 100$/total moles of products.

[d] Percentage of selectivity with respect to butanes and butenes, moles of $C_4 \times 100$/total moles of products.

[e] Molar ratio of isobutane/*n*-butane.

[f] Molar ratio olefins/parafins in the C_2 to C_4 range.

[g] Activated in a methane flow of 10 cm^3/min at 600°C for 8 h. 1 h of reaction at 350°C, GHSV = 565 h^{-1}.

[h] Activated in a methane flow of 10 cm^3/min at 600°C for 8 h. 1 h of reaction at 350°C, GHSV = 968 h^{-1}.

[i] Activated in a hydrogen flow of 10 cm^3/min at 300°C for 8 h. 1 h of reaction at 350°C, GHSV = 968 h^{-1}.

[j] No *n*-butane was detected.

[k] GHSV = 1548 h^{-1}, no ethylene present.

der the hydrogen atmosphere (Experiment 5) the formation of butanes decreased from 81.4 to 51.7% in comparison with the methane-activated reaction (Experiment 3). The difference in catalytic activity can be attributed to a concentration of the proposed active phase (C_1 species) relatively lower in the former than in the latter experiment. Schleyer and co-workers (*6*) reported a similar effect but at 10 atm of pressure.

When the reaction of propene and hydrogen was carried out in the absence of methane (Experiment 6), 32.3% of butanes and butenes was obtained using a CH_4-activated catalyst. This finding may suggest an alternative mechanism for the generation of the C_4 products in which the CH_4 molecule acts as a hydrogen source (Eq. (3)). The promoting effects of hydrogen in the homologation reaction are well documented in the literature (*15, 16, 21, 22*):

$$CH_4 \rightarrow CH_x + H_2, \quad \text{where } x = 0, 1, 2, 3. \quad (3)$$

As reported by Strehlow and Douglas (*22*), there is a competition between the hydrogenation and the homologation reactions as can be seen in Table 1; i.e., the selectivity to C_4 compounds increases as the selectivity to propene decreases for all the experiments shown. However, by comparing Experiments 5 and 6 it can be observed that for the same hydrogenation activity (approximately 48%), the selectivity to C_4 compounds is greater for the methane-containing reaction (52.7%) than for the hydrogen-containing analog (32.3%). This result clearly indicates that methane is incorporated into the hydrocarbon chain to generate the homologation products, as also reported by Schleyer and co-workers (*6*).

In order to determine the difference of activity for the alumina- and silica-supported catalysts, a surface characterization study was undertaken and the results are discussed in the next section.

Characterization of the Catalysts

The results of the X-ray photoelectron spectroscopy study for the alumina-supported nickel catalyst are shown in Tables

TABLE 2

Nickel (Ni $2p_{3/2}$) XPS Bands for the Alumina-Supported Catalysts[a]

Treatment	B.E.[b]	B.E.[c]	Area[d]	% A_t[e]	Assignment
Calcined in air at 600°C[f]	860.7	855.44	5.88×10^3	3.46	Ni^{2+}
	866.72	861.35	3.09×10^3		(NiO and $NiAl_2O_4$)
Activated CH_4 at 600°C[g]	852.87	852.87	2.58×10^2	0.18	Ni^0 associated with conductive phase
	857.35	851.2	4.79×10^2		Ni^{2+} ($NiAl_2O_4$)
	861.7	855.55	7.6×10^1		
Reaction $CH_4 + C_3H_6$[h]	857.69	852.15	1.03×10^3	1.16	Ni^0 associated with the support with charge effect
	861.16	855.62	2.05×10^3		Ni^{2+} (Most probably
	866.78	861.24	7.51×10^2		$NiAl_2O_4$)

[a] Catalyst prepared by incipient wetness technique.
[b] Binding energy taken from the spectrum in eV.
[c] Binding energy corrected by charge effect in eV.
[d] Peak area (arbitrary units).
[e] Nickel atomic percentage including the support.
[f] Catalyst calcined in air for approximately 16 h.
[g] Catalyst activated in a methane flow of 10 cm^3/min for 8 h.
[h] After 1 h of reaction time with 9% of propene in the gas feed GHSV = 38 h^{-1}. reaction temperature of 350°C, catalyst activated as in footnote g.

2 to 5. In these tables the binding energies for the Ni and the carbon obtained from the XPS measurements are presented (uncorrected and corrected for the charge effect). The relative areas, the surface atomic percentages, and the most probable assignments are also shown.

For the air-calcined catalyst, a band at 855.44 eV attributed to Ni^{2+} is observed with its corresponding satellite at 861.35 eV (Table 2). For the Ni $2p_{3/2}$ main peak, Shalvoy and co-workers reported (*23*) values of 854.6 and 856.1 eV corresponding to NiO/Al_2O_3 and $NiAl_2O_4$, respectively. In addition, the value registered for pure NiO is in the range 854–855 eV (*24*). Hence, the presence of nickel oxide on the surface of the Ni/Al_2O_3 catalyst calcined in air at 600°C can be proposed. However, the presence of $NiAl_2O_4$ cannot be ruled out on the basis of the XPS data alone.

For the alumina catalyst activated under the methane atmosphere, the percentage of atomic nickel present on the surface decreased from 3.46 to 0.18% in comparison with the calcined catalyst (Table 2). On the other hand, the carbon percentage increased from 9.4 (adventitious carbon) to almost 80% (Table 3). This result is not surprising because, in general, the activation of a catalyst under a methane atmosphere produces carbon deposits which, in some cases, are reported to be the catalytic active species (*25*). Thus, the surface of the Ni/Al_2O_3 catalyst can be described as being approximately 80% covered by a carbonaceous layer.

As reported in the literature (*23, 24*), the determination of the correction factor due to charge effect is generally performed using the adventitious carbon (284.6 eV) as reference. For the Ni/Al_2O_3 catalyst three bands are observed in the carbon region (Table 3), which made this calculation difficult. For this reason, the aluminum band of the calcined catalyst at 74.09 eV (Table 4) is chosen

TABLE 3

Carbon (C 1*s*) XPS bands for the Alumina-Supported Nickel Catalysts[a]

Treatment	B.E.[b]	B.E.[c]	Area[d]	% A_i[e]	Assignment
Calcined in air at 600°C[f]	287.38	282.08	6.09×10^2	9.39	
	289.9	284.60	8.36×10^2		Adventitious carbon
	292.2	286.90	2.59×10^2		
Activated CH_4 at 600°C[g]	284.58	284.58	4.86×10^3	79.56	Adventitious carbon
	285.47	285.47	3.15×10^3		and conducting phase
	289.57	289.57	2.52×10^3		
Reaction $CH_4 + C_3H_6$[h]	285.94	280.40	9.20×10^2	15.38	Metallic carbide
	285.94	284.60	2.64×10^3		Adventitious carbon

[a] Catalyst prepared by incipient wetness technique.
[b] Binding energy taken from the spectrum in eV.
[c] Binding energy corrected by charge effect in eV.
[d] Peak area (arbitrary units).
[e] Carbon atomic percentage including the support.
[f] Catalyst calcined in air for approximately 16 h.
[g] Catalyst activated in a methane flow of 10 cm^3/min for 8 h.
[h] After 1 h of reaction time with 9% of propene in the gas feed GHSV = 38 h^{-1}, reaction temperature of 350°C, catalyst activated as in footnote g.

and a correction factor for the methane-activated catalyst of 6.15 eV is calculated. By subtracting this factor from the binding energies of the Ni $2p_{3/2}$ at 852.87 eV (Table 2) and the O 1*s* at 532.49 eV (Table 5), it is found that the corrected values are significantly lower than those reported in the literature for similar alumina-supported nickel catalysts (*23–26*). Therefore, those bands are assigned to Ni^0 and O^{2-} species associated with a carbonaceous conducting phase on the catalyst surface and are not shifted

TABLE 4

Aluminum (Al 2*p*) XPS Bands for the Alumina-Supported Nickel Catalysts[a]

Treatment	B.E.[b]	B.E.[c]	Area[d]	% A_i[e]	Assignment
Calcined in air at 600°C[f]	79.39	74.09	3.59×10^3	38.45	Al^{3+} of the alumina
Activated CH_4 at 600°C[g]	80.24	74.09	5.26×10^2	7.72	Al^{3+} of the alumina
Reaction $CH_4 + C_3H_6$[h]	79.07	74.09	4.73×10^3	39.77	Al^{3+} of the alumina

[a] Catalyst prepared by incipient wetness technique.
[b] Binding energy taken from the spectrum in eV.
[c] Binding energy corrected by charge effect in eV.
[d] Peak area (arbitrary units).
[e] Aluminum atomic percentage including the support.
[f] Catalyst calcined in air for approximately 16 h.
[g] Catalyst activated in a methane flow of 10 cm^3/min for 8 h.
[h] After 1 h of reaction time with 9% of propene in the gas feed GHSV = 38 h^{-1}, reaction temperature of 350°C, catalyst activated as in footnote g.

TABLE 5

Oxygen (O 1*s*) XPS Bands for the Alumina-Supported Nickel Catalysts[a]

Treatment	B.E.[b]	B.E.[c]	Area[d]	% A_t[e]	Assignment
Calcined in air at 600°C[f]	536.12	530.82	2.68×10^4	48.7	O^{2-} of the alumina
Activated CH_4 at 600°C[g]	532.49	532.49	1.28×10^3	12.54	O^{2-} of the alumina associated with the conducting phase
	536.69	530.54	3.76×10^3		O^{2-} of the alumina
Reaction $CH_4 + C_3H_6$[h]	536.31	530.77	3.06×10^4	43.68	O^{2-} of the alumina

[a] Catalyst prepared by incipient wetness technique.
[b] Binding energy taken from the spectrum in eV.
[c] Binding energy corrected by charge effect in eV.
[d] Peak area (arbitrary units).
[e] Oxygen atomic percentage including the support.
[f] Catalyst calcined in air for approximately 16 h.
[g] Catalyst activated in a methane flow of 10 cm^3/min for 8 h.
[h] After 1 h of reaction time with 9% of propene in the gas feed GHSV = 38 h^{-1}, reaction temperature of 350°C, catalyst activated as in footnote g.

by charge effect (Tables 2 and 5). On the other hand, the other two bands in the nickel XPS spectrum at 851.2 and 855.55 eV are attributed (*23, 24*) to Ni^0 associated with the support and are registered in Table 2 with charge effect.

Because, as mentioned before, 80% of the catalyst surface is covered by carbon, a carbonaceous conducting phase produced by the methane treatment is not surprising; thus, the bands in Table 3 attributed to C 1*s* are also not shifted and are reported at the same value found in the XPS spectrum.

When the reaction of methane with propene is carried out at 350°C for an hour, the atomic carbon percentage decreases from 80 to 15%. The immediate result is the absence of the carbonaceous conducting phase similar to the one discussed previously. When the charge effect is substracted, all the binding energies corresponding to nickel, aluminum, and oxygen (Tables 2, 4, and 5, respectively) are registered in the correct intervals, as reported in the literature (*23–26*). Two species of nickel that correspond to Ni^0 and Ni^{2+} can be detected. The presence of the latter species can be attributed to the removal of the carbonaceous conducting phase which exposed unreduced Ni^{2+} metal ions.

For the latter catalyst, the carbonaceous species with a binding energy of 280.40 eV (Table 3) can be assigned to nickel carbide. Values for the WC, TiC, and HfC binding energies (corresponding to C 1*s*) of 282.6, 281.1, and 280.6 eV, respectively, are reported in the literature (*24*). No previous reference is found for the NiC, but, in general, the metal carbide XPS spectrum has (*24*) binding energies lower than that of the adventitious carbon (284.6 eV).

The results of the X-ray photoelectron spectroscopy study for the silica-supported nickel catalyst are shown in Tables 6 to 9. For the calcined catalyst two bands assigned (main peak and satellite) for a Ni^{2+} species are found (Table 6). On the other hand, the nickel atomic percentage is higher in the silica catalyst than in the alumina-supported analog (35% vs 3.5%, respectively). This difference can be attributed to a lower interaction of the metal with the support in the former catalyst than in the latter.

For the calcined catalyst, the band at

TABLE 6

Nickel (Ni $2p_{3/2}$) XPS Bands for the Silica-Supported Catalysts[a]

Treatment	B.E.[b]	B.E.[c]	Area[d]	% A_t[e]	Assignment
Calcined in air at 600°C[f]	855.98	854.27	2.90×10^4	35.47	Ni^{2+}
	862.05	860.34	2.27×10^4		
Activated CH_4 at 600°C[g]	852.58	852.58	1.92×10^2	0.14	Ni^0 associated with conducting phase
	855.39	852.26	1.38×10^2		Ni^0 associated with
	859.61	856.48	5.8×10^1		the support with charge effect
Reaction $CH_4 + C_3H_6$[h]	854.94	854.94	1.76×10^3	9.03	Ni^0 associated with conducting phase
	858.17	852.94	5.08×10^3		Ni^0 associated with the support with charge effect
	861.16	855.93	8.98×10^3		Ni^{2+}
	866.33	861.10	3.09×10^3		

[a] Catalyst prepared by incipient wetness technique.
[b] Binding energy taken from the spectrum in eV.
[c] Binding energy corrected by charge effect in eV.
[d] Peak area (arbitrary units).
[e] Nickel atomic percentage including the support.
[f] Catalyst calcined in air for approximately 16 h.
[g] Catalyst activated in a methane flow of 10 cm^2/min for 8 h.
[h] After 1 h of reaction time with 9% of propene in the gas feed GHSV = 968 h^{-1}, reaction temperature of 350°C, catalyst activated as in footnote g.

TABLE 7

Carbon (C 1*s*) XPS bands for the Silica-Supported Nickel Catalysts[a]

Treatment	B.E.[b]	B.E.[c]	Area[d]	% A_t[e]	Assignment
Calcined in air at 600°C[f]	286.31	284.60	1.70×10^3	18.0	Adventitious carbon
	289.75	288.04	1.34×10^2		
Activated CH_4 at 600°C[g]	284.54	284.54	1.35×10^4	97.39	Adventitious carbon
	286.37	286.37	1.69×10^3		and conducting
	289.35	289.35	3.86×10^3		phase
Reaction $CH_4 + C_3H_6$[h]	285.54	285.54	5.02×10^3	59.04	Adventitious carbon
	290.10	290.10	3.65×10^3		and conducting phase

[a] Catalyst prepared by incipient wetness technique.
[b] Binding energy taken from the spectrum in eV.
[c] Binding energy corrected by charge effect in eV.
[d] Peak area (arbitrary units).
[e] Carbon atomic percentage including the support.
[f] Catalyst calcined in air for approximately 16 h.
[g] Catalyst activated in a methane flow of 10 cm^3/min for 8 h.
[h] After 1 h of reaction time with 9% of propene in the gas feed GHSV = 968 h^{-1}, reaction temperature of 350°C, catalyst activated as in footnote g.

TABLE 8

Silicon (Si 2*p*) XPS Bands for the Silica-Supported Nickel Catalysts[a]

Treatment	B.E.[b]	B.E.[c]	Area[d]	% A_t[e]	Assignment
Calcined in air at 600°C[f]	105.47	103.76	4.91×10^2	6.1	Si^{4+} of the silica
Activated CH_4 at 600°C[g]	106.89	103.76	8.0×10^1	0.72	Si^{4+} of the silica with charge effect
	104.29	104.29	3.0×10^1		Si^{4+} of the silica associated with the conducting phase
Reaction $CH_4 + C_3H_6$[h]	108.99	103.76	8.48×10^2	7.33	Si^{4+} of the silica with charge effect

[a] Catalyst prepared by incipient wetness technique.
[b] Binding energy taken from the spectrum in eV.
[c] Binding energy corrected by charge effect in eV.
[d] Peak area (arbitrary units).
[e] Silicon atomic percentage including the support.
[f] Catalyst calcined in air for approximately 16 h.
[g] Catalyst activated in a methane flow of 10 cm^3/min for 8 h.
[h] After 1 h of reaction time with 9% of propene in the gas feed GHSV = 968 h^{-1}, reaction temperature of 350°C, catalyst activated as in footnote g.

103.76 eV (Si 2*p*) attributed to the Si^{4+} of the support is used as a reference (Table 8) in order to calculate the charge effect for the methane-activated silica catalyst. For the latter catalyst and for the Ni $2p_{3/2}$ three bands are observed and attributed to two Ni^0 species on the surface (Table 6). Using the same arguments as for the alumina analog, the band at 852.58 eV is assigned to metallic nickel associated with the carbonaceous conducting phase; thus, this value of binding energy is not corrected for charge effect as depicted in Table 6. The other Ni^0 species does exert this effect and it is shown at 852.26 and 856.48 eV for the main peak and its satellite, respectively. These binding energies are in the range reported in the literature for nickel-supported catalysts (*23–26*). It is important to note that the atomic carbon percentage for this catalyst is 97% (Table 7); thus, the presence of a conducting phase due to the carburization process can be safely proposed.

For the Ni/SiO_2 catalyst used in the methane–propene reaction the atomic carbon percentage is 60% (Table 7). The charge effect calculated using the Si 2*p* (assuming a conducting carbonaceous phase) allows the identification of three nickel species over the catalyst surface (Table 6). The first, at 854.94 eV, is assigned to Ni^0 associated with the conducting phase and is not detected on the Ni/Al_2O_3 catalyst treated under the same conditions. The other two with charge effect are Ni^0 associated with the support (at 852.94 eV) and Ni^{2+}, produced by the removal of approximately 40% of the carbonaceous phase, at 855.93 eV with its corresponding satellite at 861.1 eV.

For the activated and the used catalysts two peaks are found for the O 1*s* (Table 9). These bands are attributed to O^{2-} species associated either with the conducting carbonaceous phase or with the anion of the silica carrier with its corresponding charge effect.

As previously shown, the binding energies for the conducting carbonaceous phase for the silica and alumina catalysts are in the range 284–290 eV. For both cases the

TABLE 9

Oxygen (O 1*s*) XPS Bands for the Silica-Supported Nickel Catalysts[a]

Treatment	B.E.[b]	B.E.[c]	Area[d]	% A_i[e]	Assignment
Calcined in air at 600°C[f]	530.93	529.22	8.65×10^3	40.43	O^{2-} of the silica
	533.88	532.17	3.89×10^3		
Activated CH_4 at 600°C[g]	533.88	530.25	7.49×10^2	1.75	O^{2-} of the silica
	536.41	533.28	2.91×10^2		
Reaction $CH_4 + C_3H_6$[h]	535.33	530.10	5.78×10^3	24.59	O^{2-} of the silica
	537.83	532.60	5.17×10^3		

[a] Catalyst prepared by incipient wetness technique.
[b] Binding energy taken from the spectrum in eV.
[c] Binding energy corrected by charge effect in eV.
[d] Peak area (arbitrary units).
[e] Oxygen atomic percentage including the support.
[f] Catalyst calcined in air for approximately 16 h.
[g] Catalyst activated in a methane flow of 10 cm^3/min for 8 h.
[h] After 1 h of reaction time with 9% of propene in the gas feed GHSV = 968 h^{-1}, reaction temperature of 350°C, catalyst activated as in footnote g.

presence of CH_x, where $x = 0$, 1, 2, or 3, cannot be discounted because the C 1*s* band is also reported in that range (*24*). The role of these species in the activation of methane as well as in the homologation of propene is discussed later.

Metal Dispersions and Magnetic Susceptibility Studies

In general, metal dispersions are calculated by dividing the atomic percentages of the metal into those corresponding to the support (Al or Si oxides). However, for the methane-activated catalysts, the signals corresponding to the elements on the surface are attenuated by the carbonaceous layer (Tables 3 and 7). In order to determine the real values of the metal dispersions, the correct intensities can be calculated using

$$I_A^0 = I_A e^{a/\lambda_A}, \qquad (4)$$

where

I_A^0 is the corrected intensity of element A
I_A is the intensity of element A
a is the width of the carbonaceous layer
λ_A is the mean free path of the electron emitted from element A in the carbon layer.

The width of the carbonaceous layer (a) can be calculated by determining (using XPS) the carbon atomic percentage on the surface, and the mean free path by the relative energies of the emitted electrons from the element A and the carbon (*27*).

Using this procedure, the dispersions of the nickel with respect to the support (Al or Si) can be calculated and are shown in Table 10. As can be seen, there are significant differences between the dispersion measured from the intensities of the XPS spectra and the corrected values using Eq. (4). For example, when the carbon percentage is high (between 60 and 97%) the greatest differences are observed. In particular, for the methane-activated Ni/SiO_2 catalyst the calculated and corrected dispersions are 0.194 and 1.45, respectively, showing an increase in one order of magnitude.

For the alumina and silica catalysts, the metal dispersions decrease after the activation procedure but remain approximately constant after the reaction with propene and methane. However, the dispersion of the silica catalyst is considerably greater than that found for the alumina analog (two orders of magnitude). The effect of the disper-

TABLE 10

Metal Dispersions and Average Particle Size Measured by Magnetic Susceptibility for the Nickel-Supported Catalysts[a]

Catalyst	Treatment	Dispersion by XPS[b]	Corrected dispersion[c]	% Atomic carbon[d]	Particle size (Å)[e]
Ni/Al_2O_3	Fresh	0.090	0.095	9.39	—
Ni/Al_2O_3[f]	CH_4	0.023	0.059	79.56	32.7
Ni/Al_2O_3[f,g]	$CH_4 + C_3H_6$	0.029	0.032	15.38	31.8
Ni/SiO_2	Fresh	5.81	6.57	18.0	—
Ni/SiO_2[f]	CH_4	0.194	1.45	97.39	42.3
Ni/SiO_2[f,g]	$CH_4 + C_3H_6$	1.23	2.06	59.04	43.4

[a] Catalyst prepared by incipient wetness technique.
[b] Defined as the ratio of the atomic percentage of Ni/atomic percentage of Al or Si, measured by XPS.
[c] Defined as the ratio of the atomic percentage of Ni/atomic percentage of Al or Si, corrected from the top carbon layer. For details see text.
[d] Atomic percentage of carbon as in Tables 3 and 7.
[e] Average particle size measured by magnetic susceptibility as reported by Sinfelt and Carter (*11*).
[f] Activated in a methane flow of 10 cm^3/m at 600°C for 8 h.
[g] One-hour reaction time at 350°C, 9% of propene in methane.

sion of the metal on the catalytic activity is discussed next.

As reported by Sinfelt and Carter (*11*) and Mulay and Yamamura (*28*), the approximate size of metal particles in alumina- and silica-supported nickel catalysts can be calculated by plotting the square of the magnetization per gram of sample versus the intensity of the applied magnetic field and using the values of the slope at low field. The plots are shown in Figs. 4 and 5 and in Table 10. As can be seen, the nickel particle sizes for the alumina and silica catalysts are approximately of the same radius with values of 30 and 40 Å, respectively. As the percentage of nickel in both catalysts is nominally the same, and the metal dispersion of the Ni/SiO_2 catalyst is 100 times greater than that found for the alumina analog, it can be concluded that most of the metal in the latter is not available for the homologation reaction and it is present, most probably, in the form of nickel aluminate in the bulk of the solid. In the case of the silica catalyst, the metal

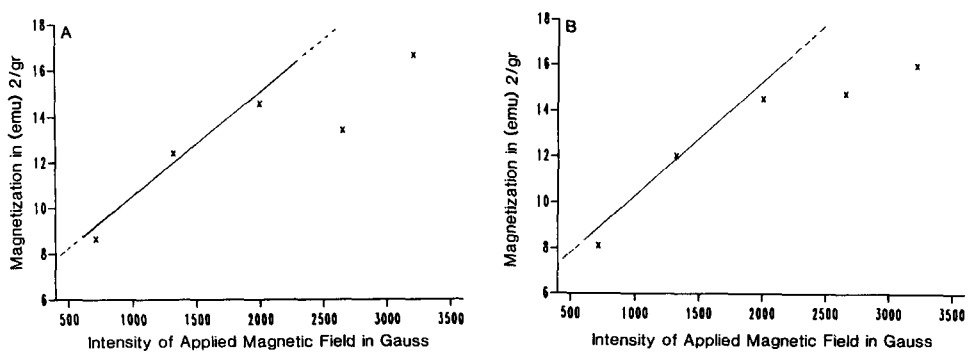

FIG. 4. Plots of the square of the magnetization per gram of catalyst versus the intensity of the applied magnetic field for the Ni/Al_2O_3 catalyst. (A) Methane-activated catalyst. (B) After the propene–methane reaction.

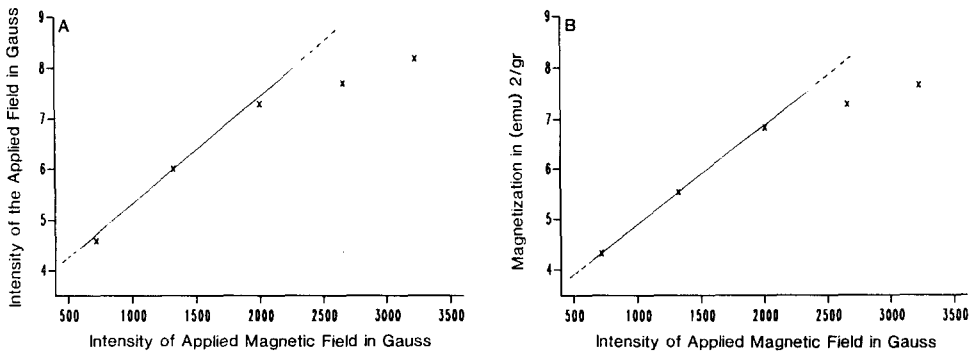

FIG. 5. Plots of the square of the magnetization per gram of catalyst versus the intensity of the applied magnetic field for the Ni/SiO_2 catalyst. (A) Methane-activated catalyst. (B) After the propene–methane reaction.

remains on the surface and the production of butanes is enhanced. This may account for the differences in catalytic activity as discussed previously (Table 1).

Proposed Mechanism for Propene Homologation

On the basis of all the evidence presented, a mechanism for the homologation of propene with methane can be proposed and is shown in Fig. 6. In the first step, the nickel on the surface reacts with methane to generate species $Ni–CH_x$, where $x = 0, 1, 2,$ or 3. This reaction was mentioned in the Introduction and has been reported (*29*) for metals with high *d* character. The effect on the butane selectivity of substituting methane with nitrogen indicates that the former is definitely involved in the olefin homologation reaction. The lower activity shown by the Ni/Al_2O_3 system demonstrated that the presence of the metal, at relatively higher concentration, on the catalyst surface is necessary in order to achieve an effective activation of methane and also to regenerate the active carbonaceous layer. In turn, this layer reacts with the olefin to give the homologation products. As mentioned, the Ni/SiO_2 catalyst has higher metal dispersion and is, therefore, active for the synthesis of C_4 compounds.

The $Ni–CH_x$ species proposed in Fig. 6 can exist on the carbonaceous layer detected on the catalyst surface after the activation period and after the reaction with propene and methane. These results are in accord with those published by Somorjai and Zaera (30) in which an active carbonaceous (but not necessarily graphitic) layer on the surface of a platinum-reforming catalyst was proposed. On the other hand, the lower selectivity for butanes found using hydrogen-activated catalyst (Experiment 5, Table 1) indicates that the formation of this carbonaceous layer favors the incorporation of methane. Other evidence for the existence of the active $Ni–CH_x$ species is that methane is detected when a Ni/SiO_2 catalyst (previously activated in CH_4 at 600°C for 6 h) is exposed to an atmosphere of hydrogen at 200°C.

Finally, a mechanism that involves reac-

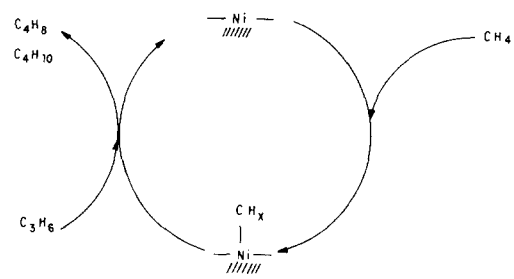

FIG. 6. Proposed mechanism for the homologation of propene with methane using nickel-supported catalysts (where $x = 0, 1, 2,$ or 3).

tion of the CH_x species with propene to generate the homologation products was also proposed by Basset and co-workers (*31*) in their studies of formation of the C_6 compounds by reaction of a C_1 species with 1-pentene using silica-supported ruthenium catalyst.

CONCLUSIONS

• Experiments carried out using a propene/methane mixture at 350°C showed that the Ni/SiO_2 system was more active for the homologation reaction (81.4% selectivity to butanes) than its alumina analog (6.2% selectivity to C_4 compounds). From control experiments carried out under a nitrogen atmosphere and in hydrogen-activated catalyst, it was concluded that the methane molecule incorporates into the hydrocarbon chain.

• The results of the XPS studies showed that concentrations of carbonaceous (but not necessarily graphitic) species present on the surface of the silica catalyst were higher than those found in its alumina analog, suggesting that, most probably, these species are involved as intermediates in the propene homologation reaction.

• The silica-based catalyst shows metal dispersion higher than that found in its alumina counterpart. This can be attributed to the formation of $NiAlO_4$ on the catalyst surface, which can also explain the lower activity observed for butane production.

• A propene homologation mechanism is proposed involving the reaction of methane with the metal to generate CH_x species (where $x = 0, 1, 2,$ or 3), which in turn reacts with propene to produce the homologation products (butanes).

REFERENCES

1. Pitchai, R., and Klier, K., *Catal. Rev. Sci. Eng.* **28,** 13 (1986).
2. Lee, J. S., and Oyama, S. T., *Catal. Rev. Sci. Eng.* **30,** 249 (1988).
3. Scurrel, M. S., *Appl. Catal.* **32,** 1 (1987).
4. Anderson, J. R., *Appl. Catal.* **47,** 176 (1989).
5. Mimoun, H., *Nouv. J. Chim.* **11,** 513 (1987),
6. Schleyer, P. R. J., Loffler, I. D., Maier, W. F., and Andrade, J. G., *J. Chem. Soc. Chem. Commun.*, 1178 (1984).
7. Sodesawa, T., Matsubara, M., Satoh, S., and Nozaki, F., *Chem. Lett.*, 1513 (1987).
8. Scurrell, M. S., *Appl. Catal.* **34,** 109 (1987).
9. Osada, Y., Enomoto, K., Fukushima, T., Ogasawara, S., Shikada, T., and Ikariya, T., *J. Chem. Soc. Chem. Commun.*, 1156 (1989).
10. Leon, V., and Carrazza, J., *Rev. Tec. INTEVEP* **9,** 81 (1989).
11. Sinfelt, J. H., and Carter, J. L., *J. Phys. Chem.* **79,** 3003 (1966).
12. Ovalles, C., Leon, V., Reyes, S, and Rosa, F., Report No. INT -02113,89, INTEVEP, S. A., Los Teques, Venezuela, 1989.
13. Dry, M. E., *Catal. Sci. Tech.* **1,** 159 (1981).
14. Tanaka, K., and Tanaka, K-i, *J. Chem. Soc. Faraday Trans. 1* **83,** 1859 (1987).
15. O'Donohoe, C., Clarke, J. K. A., and Rooney, J. J., *J. Chem. Soc. Faraday Trans. 1* **76.** 345 (1980).
16. O'Neill, P. P., and Rooney, J. J., *J. Am. Chem. Soc.* **94,** 4383 (1972).
17. Hugues, F., Besson, B., and Basset, J. M., *J. Chem. Soc. Chem. Commun.*, 791 (1980).
18. Theolier, L. A., Rojas, D., and Basset, J. M., *J. Am. Chem. Soc.* **106,** 1141 (1984).
19. Hughes, F., Besson, B., Bussiere, P., Dalmon, J. A., Basset, J. M., and Olivier, D., *Nouv. J. Chim.* **5,** 207 (1981).
20. Iisawa, Y., and Yamada, M., *J. Chem. Soc. Chem. Commun.*, 1895 (1980).
21. Yamaguchi, R., Nakamura, S., and Tanabe, K., *J. Chem. Soc. Chem. Commun.*, 621 (1982).
22. Strehlow, R., and Douglas, E., *J. Chem. Soc. Chem. Commun.*, 259 (1983).
23. Shalvoy, R. B., Davis, B. H., and Reucroft, P. J., *Surf. Interface Anal.* **2,** 11 (1980).
24. "Handbook of X-Ray Photoelectronic Spectroscopy," Perkin–Elmer Corporation, 1979.
25. Briggs, D., and Seah, M. P., "Practical Surface Analysis by Auger and X-Ray Photoelectron Spectroscopy." Wiley, New York, 1986.
26. Wagner, C. D., Gale, L. H., and Raymond, R. H., *Anal. Chem.* **51,** 466 (1979).
27. Leon, V., and De Jesus, J. C. Submitted for publication.
28. Mulay, L. N., and Yamamura, H., *J. Appl. Phys.* **50,** 7795 (1979).
29. Frennet, A., *Catal. Rev. Sci. Eng.* **10,** 37 (1974).
30. Somorjai, G. A., and Zaera, F., *J. Phys. Chem.* **86,** 3070 (1982).
31. Basset, J. M., Rodriguez, E., Leconte, M., and Tanaka, K. I., *J. Am. Chem. Soc.* **110,** 275 (1988).